PHARMACIA

Pharmacia 72: 1–11
DOI 10.3897/pharmacia.72.e143171

Research Article

Synthesis, molecular docking, and anti-inflammatory evaluation of novel 4-(benzo[*d*][1,3]dioxol-5-yloxy)-*N*,*N*-2-yn-1-amine derivatives as potent cysteinyl leukotriene receptor (CysLT2) antagonists

Areej M. Jaber[1], Mohammed M. Al-Mahadeen[2], Belal O. Al-Najjar[1,3], Raed A. Al-Qawasmeh[4]

1 *Pharmacological and Diagnostic Research Center, Faculty of Pharmacy, Al-Ahliyya Amman University, Amman 19328, Jordan*
2 *Chemistry Department, Faculty of Science, The University of Jordan, Amman, 11942, Jordan*
3 *Pharmaceutical Sciences Department, Faculty of Pharmacy, Al-Ahliyya Amman University, Amman 19328, Jordan*
4 *Pure and Applied Chemistry Group, Department of Chemistry, College of Sciences, University of Sharjah, Sharjah 27272, United Arab Emirates*

Corresponding author: Areej M. Jaber (a.jaber@ammanu.edu.jo)

Received 30 November 2024 ♦ **Accepted** 12 February 2025 ♦ **Published** 28 February 2025

Citation: Jaber AM, Al-Mahadeen MM, Al-Najjar BO, Al-Qawasmeh RA (2025) Synthesis, molecular docking, and anti-inflammatory evaluation of novel 4-(benzo[*d*][1,3]dioxol-5-yloxy)-*N*,*N*-2-yn-1-amine derivatives as potent cysteinyl leukotriene receptor (CysLT2) antagonists. Pharmacia 72: 1–11. https://doi.org/10.3897/pharmacia.72.e143171

Abstract

Cysteinyl leukotrienes (CysLTs), derived from arachidonic acid, play a crucial role in regulating inflammation. We synthesized a novel series of CysLT2 antagonists containing the benzo[*d*][1,3]dioxole moiety using a synthetic strategy based on the Mannich reaction, resulting in the formation of 4-(benzo[*d*][1,3]dioxol-5-yloxy)-N,N-2-yn-1-amine. The structures of the synthesized compounds were characterized through NMR and HRMS analyses, and a plausible reaction mechanism was proposed. The inhibitory activities of all new compounds against CysLT2 were evaluated in vitro. Among them, compounds **4d** and **4g** exhibited the most potent inhibitory effects, with IC_{50} values of 18.7 μM and 15.5 μM, respectively. These findings were further supported by molecular docking studies, which highlighted the binding interactions of these compounds within the kinase's active site.

Graphical abstract:

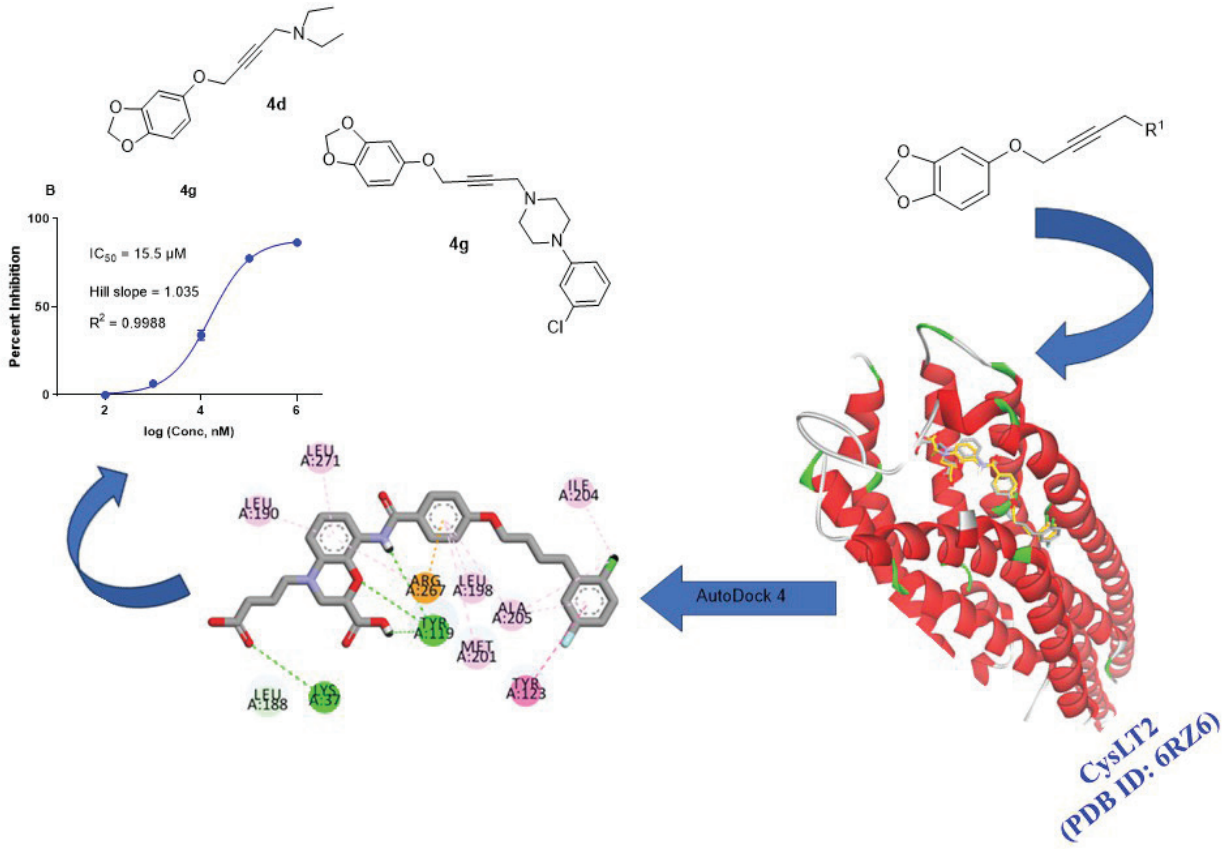

Keywords

sesamol, leukotrienes, inflammation, CysLT, Mannich reaction, allergy, asthma

Introduction

Lipid mediators called cysteineyl leukotrienes (CysLTs) are produced from arachidonic acid and are essential for the regulation of inflammation, especially in allergy and respiratory diseases. CysLTs have a major role in the development of asthma, allergic rhinitis, and other inflammatory illnesses since they are mainly responsible for bronchoconstriction, increased vascular permeability, and immune cell recruitment (Gusach et al. 2019; Sood et al. 2024). CysLTs work through certain receptors, and one of the main targets of therapeutic interventions is the CysLT2 receptor (CysLT2R). A number of intracellular signaling pathways, including those regulated by protein kinase C and phospholipase C, are connected to the CysLT2R, which causes a variety of physiological reactions that worsen bronchoconstriction and inflammation (Gelosa et al. 2017). CysLT2 receptor antagonists have become a viable treatment option for inflammatory disorders. By inhibiting CysLTs at the receptor level, these antagonists hope to lessen the pro-inflammatory effects of the protein. According to preliminary research, CysLT2 antagonists may offer therapeutic advantages over standard CysLT1 antagonists, especially in situations where CysLT2R activation plays a major role in the pathophysiology of the disease (Sekioka et al. 2015; Zhou et al. 2022). The field of CysLT2 antagonist research is still developing, with studies being conducted to learn more about the drugs' safety profiles, efficacy, and possible use in combination therapy. In the larger context of focusing on leukotriene signaling pathways to reduce inflammation and enhance outcomes in patients with respiratory and allergy disorders, this introduction emphasizes the importance of CysLT2 antagonists (Jo-Watanabe et al. 2019; Voisin et al. 2021).

Additionally, sesamol (benzo[*d*][1,3]dioxol-5-ol), a naturally occurring antioxidant present in sesame seeds, provides anti-inflammatory properties (Majdalawieh and Mansour 2019). Sesamol is a phenolic substance with a strong antioxidant capacity, and its chemical formula is $C_7H_6O_3$. It has anti-inflammatory, anticancer, cardioprotective, and neuroprotective properties in addition to being useful in the preservation of food, cosmetics, and

medications (Jayaraj et al. 2020; Kushwaha et al. 2020; Assab et al. 2024; Dayyih et al. 2024). Sesamol shields cells against oxidative stress, a factor in the emergence of chronic illnesses (Ren et al. 2018). Because both strategies concentrate on reducing the impacts of oxidative stress and inflammation, sesamol qualities complement the current research being done on CysLT2 antagonists as a means of regulating inflammation.

As part of our continuous interest in the design and discovery of new biologically active compounds (Jaber et al. 2020; Al-Mahadeen et al. 2022; Al-Mahadeen and Jaber 2024; Al-Mahadeen et al. 2024a; Al-Mahadeen et al. 2024c; Al-Mahadeen et al. 2024d; Jaber et al. 2024; Al-Mahadeen et al. 2025), we became interested in generating hybrid adducts composed of sesamol and different secondary aliphatic amines as potential lipid mediators called cysteineyl leukotrienes (CysLTs) antagonists. The synthesis of 4-(benzo[*d*][1,3]dioxol-5-yloxy)-*N*,*N*-2-yn-1-amine pharmacophore was achieved *via* copper-catalyzed Mannich reaction (Lu et al. 2019; Jaber et al. 2022; Jaber et al. 2023a; Jaber et al. 2023b; Al-Mahadeen et al. 2024b) (as in Scheme 1).

In silico profiling against several targets suggested the new compounds bind and inhibit the CysLTs antagonist (Parravicini et al. 2010; Sadybekov et al. 2020) and were therefore evaluated in vitro as CysLTs antagonists. Two of them displayed μM IC_{50} values. Interestingly, there are no previous studies on the synthesis and biological properties of these derivatives.

Materials and methods

Experimental part

Benzo[*d*][1,3]dioxol-5-ol, propargyl bromide, formaldehyde, dimethylamine, diethylamine, dipropylamine, dibutylamine, 1-methylpiperazine, 1-ethylpiperazine, 1-(3-chlorophenyl)piperazine, morpholine, 1-(2-pyridinyl)piperazine, and 2-(1-piperazinyl)pyrimidine were obtained from Acros, BLD Pharma, and Sigma-Aldrich. Nuclear magnetic resonance (NMR) spectra were recorded on a Bruker Avance III 500 MHz spectrometer, using trimethylsilane (TMS) as the internal standard. Chemical shifts (*δ*-values) were reported in parts per million (ppm), and DEPT experiments were performed to determine the carbon atom multiplicities. High-resolution mass spectra (HRMS) were acquired using a Bruker APEX IV 7 Tesla instrument, employing the electrospray ionization (ESI) technique with collision-induced dissociation. Solvents used in the study were sourced from Aldrich and BLD Pharma.

Chemistry

Synthesis and characterization of compounds (3-4a-j)

Synthesis of 5-(prop-2-yn-1-yloxy)benzo[d][1,3]dioxole (3)

This compound was prepared by the reaction of benzo[*d*][1,3]dioxol-5-ol **1** with propargyl bromide **2** in the presence of potassium carbonate in dimethylformamide according to a recently reported procedure (Chen et al. 2015).

General procedure for synthesis of compounds (4a-j)

4-(benzo[*d*][1,3]dioxol-5-yloxy)-*N*,*N*-2-yn-1-amine (4a-j)

A stirred solution of aqueous formaldehyde (35%, 1 mL) and CuI (25 mg) in 2 mL of DMSO was prepared. Alkyne **3** (0.60 mmol, 1 eq) and the appropriate amine (0.72 mmol, 1.2 eq) were then added to the solution. The reaction mixture was stirred at room temperature for 3 hours. Afterward, 8 mL of water was added, and the mixture was extracted with ethyl acetate (2 × 25 mL). The resulting residue was purified by column chromatography using a mixture of n-hexane and ethyl acetate (2:8, v/v) as the eluent to obtain compounds **4a-j**.

(benzo[*d*][1,3]dioxol-5-yloxy)-*N*,*N*-dimethylbut-2-yn-1-amine (4a)

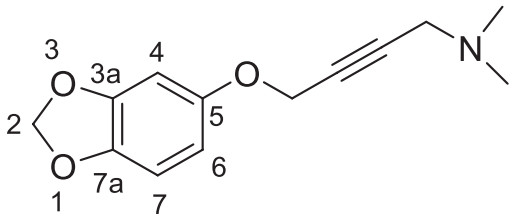

Figure 1.

Light brown oil (0.0301 g, 75% yield). **^{1}H NMR** (500 MHz, $CDCl_3$, in ppm): 2.64 (s, 6H, -CH_3), 3.37 (s, 2H, -CH_2N), 4.59 (s, 2H, -OCH_2), 5.85 (s, 2H, H-2), 6.35, 6.37 (dd, 1H, *J*= 1.5 Hz, H-6), 6.52 (s, 1H, H-4), 6.65 (d, 1H, *J*= 8.5Hz, H-7). **^{13}C NMR** (125 MHz, $CDCl_3$, in ppm): 42.1 (2C, -CH_3), 48.2 (1C, -CH_2N), 57.2 (1C, OCH_2), 79.5, 82.9 (2C, alkyne-C), 98.8 (1C, C-4), 101.2 (1C, C-2), 106.7 (1C, C-6), 107.8 (1C, C-7), 142.1 (1C, C-7a), 148.2 (1C, C-3a), 153.1 (1C, C-5). HRMS (ESI) m/z = calculated for C13H-16NO3, [M+H]+: 234.11297, found 234.11131.

4-(benzo[*d*][1,3]dioxol-5-yloxy)-*N*,*N*-diethylbut-2-yn-1-amine (4b)

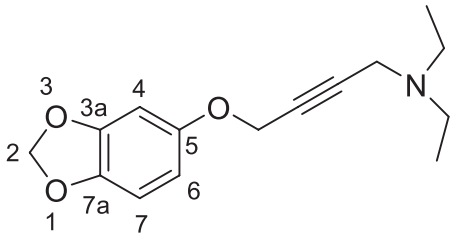

Figure 2.

Light brown oil (0.0326 g, 71% yield). **^{1}H NMR** (500 MHz, $CDCl_3$, in ppm): 1.93 (t, 6H, *J*= 7.5 Hz, -CH_2CH_3), 2.32 (t, 4H, *J*= 7.5Hz, -CH_2CH_3), 3.37 (s, 2H, -CH_2N), 4.59 (s, 2H, -OCH_2), 5.85 (s, 2H, H-2), 6.35, 6.37 (dd, 1H, *J*= 1.5 Hz, H-6), 6.52 (s, 1H, H-4), 6.65 (d, 1H, *J*= 8.5Hz, H-7). **^{13}C NMR** (125 MHz, $CDCl_3$, in ppm): 12.9 (2C, -CH_2CH_3), 42.1 (1C, -CH_2N), 49.7 (2C, -CH_2CH_3), 57.2 (1C, OCH_2), 79.5, 82.9 (2C, alkyne-C), 98.8 (1C, C-4), 101.2 (1C, C-2), 106.7 (1C, C-6), 107.8 (1C, C-7), 142.1 (1C, C-7a), 148.2 (1C, C-3a), 153.1 (1C, C-5). HRMS (ESI) m/z = calculated for C15H20NO3, [M+H]+: 263.11062, found 263.11082.

4-(benzo[*d*][1,3]dioxol-5-yloxy)-*N*,*N*-dipropylbut-2-yn-1-amine (4c)

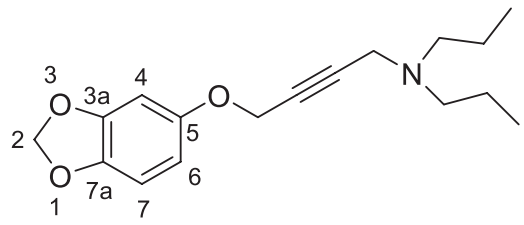

Figure 3.

Light brown oil (0.0299 g, 72% yield). **^{1}H NMR** (500 MHz, $CDCl_3$, in ppm): 0.82 (t, 6H, *J*= 7.3 Hz, -$CH_2CH_2CH_3$), 1.39 (sextet, 4H, *J*= 7.4 Hz, -$CH_2CH_2CH_3$), 2.32 (t, 4H, J= 7.5Hz, -$CH_2CH_2CH_3$), 3.37 (s, 2H, -CH_2N), 4.59 (s, 2H, -OCH_2), 5.85 (s, 2H, H-2), 6.35, 6.37 (dd, 1H, *J*= 1.5 Hz, H-6), 6.52 (s, 1H, H-4), 6.65 (d, 1H, *J*= 8.5Hz, H-7). **^{13}C NMR** (125 MHz, $CDCl_3$, in ppm): 11.9 (2C, -$CH_2CH_2CH_3$), 20.7 (2C, -$CH_2CH_2CH_3$), 42.1 (1C, -CH_2N), 55.7 (1C, OCH_2), 57.2 (2C, -$CH_2CH_2CH_3$), 79.5, 82.9 (2C, alkyne-C), 98.7 (1C, C-4), 101.2 (1C, C-2), 106.7 (1C, C-6), 107.8 (1C, C-7), 142.1 (1C, C-7a), 148.2 (1C, C-3a), 153.1 (1C, C-5). HRMS (ESI) m/z = calculated for $C_{17}H_{24}NO_3$, $[M+H]^+$: 290.17507, found 290.17485.

4-(benzo[*d*][1,3]dioxol-5-yloxy)-*N*,*N*-dibutylbut-2-yn-1-amine (4d)

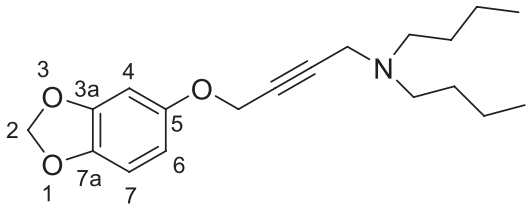

Figure 4.

Light brown oil (0.0298 g, 62% yield). **^{1}H NMR** (500 MHz, $CDCl_3$, in ppm): 0.85 (t, 6H, *J*= 7.3 Hz, -$CH_2CH_2CH_2CH_3$), 1.24 (sextet, 4H, *J*= 6.9 Hz, -$CH_2CH_2CH_2CH_3$), 1.35 (sextet, 4H, J= 7.4 Hz, -$CH_2CH_2CH_2CH_3$), 2.35 (t, 4H, *J*= 7.5 Hz, -$CH_2CH_2CH_2CH_3$), 3.37 (s, 2H, -CH_2N), 4.59 (s, 2H, -OCH_2), 5.85 (s, 2H, H-2), 6.35, 6.37 (dd, 1H, *J*= 1.5 Hz, H-6), 6.51 (s, 1H, H-4), 6.64 (d, 1H, *J*= 8.5 Hz, H-7). **^{13}C NMR** (125 MHz, $CDCl_3$, in ppm): 14.0 (2C, -$CH_2CH_2CH_2CH_3$), 20.6 (2C, -$CH_2CH_2CH_2CH_3$), 29.7 (2C, -$CH_2CH_2CH_2CH_3$), 42.1 (1C, -CH_2N), 53.5 (1C, OCH_2), 57.2 (2C, -$CH_2CH_2CH_2CH_3$), 79.6, 82.9 (2C, alkyne-C), 98.7 (1C, C-4), 101.2 (1C, C-2), 106.6 (1C, C-6), 107.8 (1C, C-7), 142.1 (1C, C-7a), 148.2 (1C, C-3a), 153.1 (1C, C-5). HRMS (ESI) m/z = calculated for $C_{19}H_{28}NO_3$, $[M+H]^+$: 318.20637, found 218.20576.

1-(4-(benzo[*d*][1,3]dioxol-5-yloxy)but-2-yn-1-yl)-4-methylpiperazine (4e)

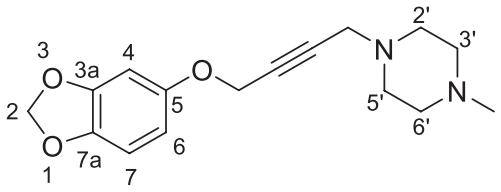

Figure 5.

Light brown oil (0.0329 g, 71% yield). **^{1}H NMR** (500 MHz, DMSO, in ppm): 2.10 (s, 3H, -NCH_3), 2.35 (ps t, 4H, H-2'/H-6'), 3.23 (s, 2H, -CH_2N), 3.31 (ps t, 4H, H-3'/H-4'), 4.68 (s, 2H, -OCH_2), 5.51 (s, 2H, H-2), 6.35, 6.37 (dd, 1H, *J*= 1.8 Hz, H-6), 6.61 (s, 1H, H-4), 6.76 (d, 1H, *J*= 8.5Hz, H-7). **^{13}C NMR** (125 MHz, $CDCl_3$, in ppm): 46.1 (1C, -NCH_3), 46.6 (1C, -CH_2N), 51.5 (2C, C-2'/C-6'), 54.9 (2C, C-3'/C-5'), 57.0 (1C, OCH_2), 80.7, 83.3 (2C, alkyne-C), 98.8 (1C, C-4), 101.5 (1C, C-2), 107.0 (1C, C-6), 108.4 (1C, C-7), 142.0 (1C, C-7a), 148.3 (1C, C-3a), 153.1 (1C, C-5). HRMS (ESI) m/z = calculated for $C_{16}H_{21}N_2O_3$, $[M+H]^+$: 288.15975, found 288.15908.

1-(4-(benzo[*d*][1,3]dioxol-5-yloxy)but-2-yn-1-yl)-4-ethylpiperazine (4f)

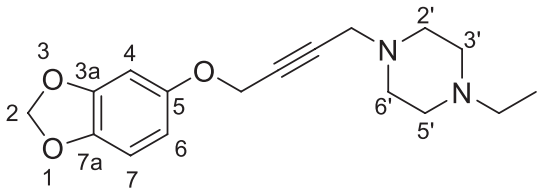

Figure 6.

Light brown oil (0.0211 g, 65% yield). **^{1}H NMR** (500 MHz, DMSO, in ppm): 1.18 (ps t, 3H, -NCH_2CH_3), 2.02 (t, 2H, *J*= 7.0 Hz, -NCH_2CH_3), 2.35 (ps t, 4H, H-2'/H-6'), 3.23 (s, 2H, -CH_2N), 3.31 (ps t, 4H, H-3'/H-4'), 4.68 (s, 2H, -OCH_2), 5.91 (s, 2H, H-2), 6.35, 6.37 (dd, 1H, *J*= 1.8 Hz, H-6), 6.61 (s, 1H, H-4), 6.76 (d, 1H, *J*= 8.5Hz, H-7). **^{13}C NMR** (125 MHz, $CDCl_3$, in ppm): 14.2 (1C, -NCH_2CH_3), 45.9 (1C, -CH_2N), 47.1 (1C, -NCH_2CH_3), 51.8 (2C, C-2'/C-6'), 54.9 (2C, C-3'/C-5'), 57.2 (1C, OCH_2), 80.1, 82.6 (2C, alkyne-C), 98.7 (1C, C-4), 101.2 (1C, C-2), 106.5 (1C, C-6), 107.9 (1C, C-7), 142.2 (1C, C-7a), 148.2 (1C,

C-3a), 153.1 (1C, C-5). HRMS (ESI) m/z = calculated for $C_{17}H_{23}N_2O_3$, $[M+Na]^+$: 325.15219, found 325.15169.

1-(4-(benzo[*d*][1,3]dioxol-5-yloxy)but-2-yn-1-yl)-4-(3-chlorophenyl)piperazine (4 g)

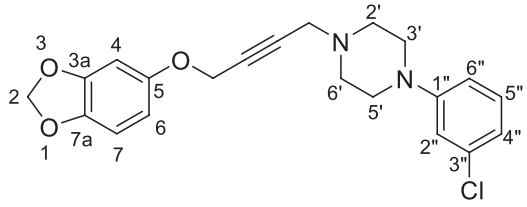

Figure 7.

Light brown oil (0.0236 g, 69% yield). **^{1}H NMR** (500 MHz, $CDCl_3$, in ppm): 2.63 (t, 4H, *J*= 4.5 Hz, H-2'/H-6'), 3.16 (t, *J*= 4.5 Hz, 4H, H-3'/H-4'), 3.35 (s, 2H, -CH_2N), 4.61 (s, 2H, -OCH_2), 5.85 (s, 2H, H-2), 6.35, 6.37 (dd, 1H, *J*= 1.2 Hz, H-6), 6.52 (s, 1H, H-4), 6.66 (d, 1H, *J*= 8.5Hz, H-7), 6.73 (d, 1H, *J*= 8.3 Hz, H-6"), 6.76 (d, 1H, *J*=8.0 Hz, H-4"), 6.83 (s, 1H, H-2"), 7.12 (t, 2H, *J*= 8.2Hz, H-5"). **^{13}C NMR** (125 MHz, $CDCl_3$, in ppm): 47.1 (1C, -CH_2N), 48.2 (2C, C-2'/C-6'), 51.7 (2C, C-3'/C-5'), 57.2 (1C, OCH_2), 80.5, 82.2 (2C, alkyne-C), 98.5 (1C, C-4), 101.2 (1C, C-2), 106.6 (1C, C-6), 107.9 (1C, C-7), 114.0 (1C, C-6"), 115.8 (1C, C-2"), 119.4 (1C, C-4"), 130.0 (1C-C-5"), 134.4 (1C, C-3"), 142.3 (1C, C-7a), 148.2 (1C, C-3a), 152.2 (1C, C-1"), 153.1 (1C, C-5). HRMS (ESI) m/z = calculated for $C_{21}H_{22}ClN_2O_3$, $[M+H]^+$: 385.13135, found 385.13300.

4-(4-(benzo[*d*][1,3]dioxol-5-yloxy)but-2-yn-1-yl)morpholine (4h)

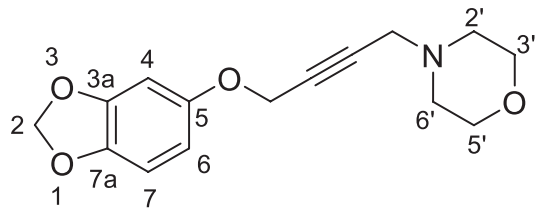

Figure 8.

Light brown oil (0.0245 g, 69% yield). **^{1}H NMR** (500 MHz, $CDCl_3$, in ppm): 2.46 (ps t, 4H, H-2'/H-6'), 3.26 (s, 2H, -CH_2N), 3.66 (ps t, 4H, H-3'/H-4'), 4.58 (s, 2H, -OCH_2), 5.56 (s, 2H, H-2), 6.33, 6.35 (dd, 1H, *J*= 1.2 Hz, H-6), 6.50 (s, 1H, H-4), 6.64 (d, 1H, *J*= 8.5Hz, H-7). **^{13}C NMR** (125 MHz, $CDCl_3$, in ppm): 47.4 (1C, -CH_2N), 52.3 (2C, C-2'/C-6'), 57.2 (2C, C-3'/C-5'), 66.8 (1C, OCH_2), 80.4, 82.3 (2C, alkyne-C), 98.7 (1C, C-4), 101.2 (1C, C-2), 106.5 (1C, C-6), 107.8 (1C, C-7), 142.2 (1C, C-7a), 148.2 (1C, C-3a), 153.1 (1C, C-5). HRMS (ESI) m/z = calculated for $C_{15}H_{18}NO_4$, $[M+H]^+$: 276.12303, found 276.12131.

1-(4-(benzo[*d*][1,3]dioxol-5-yloxy)but-2-yn-1-yl)-4-(pyridin-2-yl)piperazine (4i)

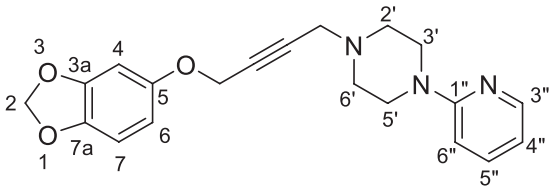

Figure 9.

Light brown oil (0.0255 g, 70% yield). **^{1}H NMR** (500 MHz, $CDCl_3$, in ppm): 2.60 (ps t, 4H, H-2'/H-6'), 3.35 (s, 2H, -CH_2N), 3.51 (ps t, 4H, H-3'/H-4'), 4.58 (s, 2H, -OCH_2), 5.83 (s, 2H, H-2), 6.33, 6.34 (dd, 1H, *J*= 2.1 Hz, H-6), 6.50 (s, 1H, H-4), 6.58 (ps t, 1H, H-7), 6.60 (br s, 1H, H-6"), 6.62 (ps t, 1H, H-4"), 7.41 (t, 1H, *J*= 7.0 Hz, H-5"), 8.13 (t, 1H, *J*= 3.2 Hz, H-3"). **^{13}C NMR** (125 MHz, $CDCl_3$, in ppm): 44.9 (2C, C-3'/C-5'), 47.1 (1C, -CH_2N), 51.6 (2C, C-2'/C-6'), 57.2 (1C, OCH_2), 80.6, 82.1 (2C, alkyne-C), 98.7 (1C, C-4), 101.2 (1C, C-2), 106.5 (1C, C-6), 107.2 (1C, C-7), 107.8 (1C, C-4"), 113.5 (1C, C-6"), 137.5 (1C, C-5"), 142.2 (1C, C-7a), 147.9 (1C, C-3"), 148.2 (1C, C-3a), 153.0 (1C, C-5), 159.3 (1C, C-1"). HRMS (ESI) m/z = calculated for $C_{20}H_{22}N_3O_3$, $[M+H]^+$: 352.16557, found 352.16380.

2-(4-(4-(benzo[*d*][1,3]dioxol-5-yloxy)but-2-yn-1-yl)piperazin-1-yl)pyrimidine (4j)

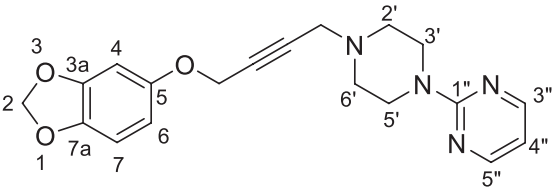

Figure 10.

Light brown oil (0.0300 g, 79% yield). **^{1}H NMR** (500 MHz, $CDCl_3$, in ppm): 2.52 (t, 4H, *J*= 4.8 Hz, H-2'/H-6'), 3.32 (s, 2H, -CH_2N), 3.78 (ps t, 4H, H-3'/H-4'), 4.55 (s, 2H, -OCH_2), 5.82 (s, 2H, H-2), 6.30, 6.31 (dd, 1H, *J*= 2.1 Hz, H-6), 6.41 (t, 1H, *J*= 4.7 Hz, H-4"), 6.47 (br s, 1H, H-4), 6.58 (d, 1H, *J*= 8.5 Hz, H-7), 8.13 (d, 2H, *J*= 4.7 Hz, H-3"/H-5"). **^{13}C NMR** (125 MHz, $CDCl_3$, in ppm): 43.3 (2C, C-3'/C-5'), 47.1 (1C, -CH_2N), 51.6 (2C, C-2'/C-6'), 57.1 (1C, OCH_2), 80.6, 82.1 (2C, alkyne-C), 98.7 (1C, C-4), 101.2 (1C, C-2), 106.5 (1C, C-6), 107.8 (1C, C-7), 109.9 (1C, C-4"), 142.2 (1C, C-7a), 148.2 (1C, C-3a), 152.9 (1C, C-5), 157.7 (2C, C-3"/C-5"), 161.1 (1C, C-1"). HRMS (ESI) m/z = calculated for $C_{19}H_{21}N_4O_3$, $[M+H]^+$: 353.16082, found 353.16102.

Biological evaluation

In vitro bioassay against cysteineyl leukotriene antagonists

CysLT2 – NFAT-bla CHO-K1: Agonist and antagonist screening protocols

Agonist screen

The bioassay followed the supplier's protocol using Invitrogen Z'-LYTE® CysLT2-NFAT-bla CHO-K1 cells. Thawed cells were resuspended in Assay Media (DMEM with 1% dialyzed FBS, 25 mM HEPES at pH 7.3, 0.1 mM NEAA, and 100 U/mL/100 µg/mL Pen/Strep) to a final concentration of 312,500 cells/mL. A volume of 32 µL (10,000 cells) was dispensed into each well of a 384-well TC-treated assay plate. The plate was incubated for 16–24 hours at 37 °C with 5% CO_2 in a humidified incubator.

Subsequently, 4 µL of a 10X serial dilution of LTD4 (control agonist, starting at 1,000 nM) or test compounds were added to the designated wells, with 4 µL of Assay Media added to bring the final volume to 40 µL per well. After a 5-hour incubation at 37 °C/5% CO_2 in a humidified incubator, 8 µL of a 1 µM Substrate + Solution D Loading Solution was added to each well. The plate was incubated at room temperature for 2 hours before fluorescence readings were taken using a plate reader.

Antagonist screen activated by LTD4

The antagonist screening utilized the same cell preparation and plating procedures as the agonist screen. Each well received 32 µL of the prepared cell suspension and was incubated for 16–24 hours at 37 °C with 5% CO_2 in a humidified incubator.

Next, 4 µL of 10X test compounds or assay media were added to the respective wells and pre-incubated with the cells for 30 minutes under the same conditions. Subsequently, 4 µL of a 10X solution of the control agonist LTD4, at its pre-determined EC80 concentration, was added to the wells containing either the control antagonist or test compounds. The plate was incubated for 5 hours at 37 °C/5% CO_2 in a humidified incubator.

Finally, 8 µL of a 1 µM substrate + solution D loading solution was added to each well, and the plate was incubated at room temperature for 2 hours. Fluorescence was measured using a plate reader. It is noted that the assay currently lacks a defined antagonist control.

Docking study

Molecular docking simulations were performed to assess the binding affinity of synthesized compounds **4d** and **4g** to the CysLT2 receptor (PDB ID: 6RZ6) (Gusach et al. 2019). The simulations were conducted using AutoDock 4.2.6 (Morris et al. 2009), following previously established protocols from our group (Al-Anazi et al. 2022; Sahar Jaffal 2022). Protein preparation was carried out in BIOVIA® Discovery Studio® 16.1 (Dassault-Systèmes 2016), which involved removing water molecules and co-crystallized structures. The co-crystallized antagonist (Compound **11a**) (Gusach et al. 2019) (Fig. 11) was extracted from the crystal structure to serve as the control ligand.

AutoDockTools 1.5.6 (Morris et al. 2009) was used to prepare the protein by adding Kollman charges and polar hydrogens, while Gasteiger charges were applied to the optimized ligand structures. A grid box with dimensions

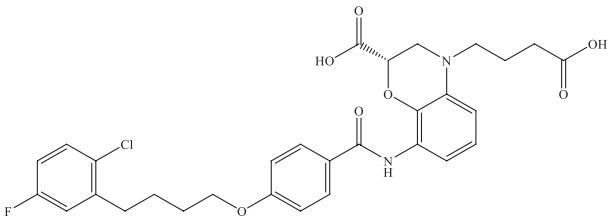

Figure 11. 2D Chemical structure of the co-crystalized antagonist (compound **11a**) from (PDB ID: 6RZ6). Generated by ChemDraw® software.

of 16.453 Å^3 and coordinates set at -23.401 (x), 11.66 (y), and -20.827 (z) was defined. Docking simulations were executed using 100 runs of the Lamarckian genetic algorithm with default parameters.

Conformations with the lowest binding free energy (LEB) and the highest cluster populations were selected for further analysis. Interaction analyses were conducted using BIOVIA® Discovery Studio® 16.1 to explore ligand-receptor interactions.

Results and discussion

Chemistry

In this work, a number of 4-(benzo[*d*][1,3]dioxol-5-yloxy)-*N*,*N*-2-yn-1-amine compounds were synthesized and identified. Benzo[*d*][1,3]dioxol-5-ol **1** was first intended to be linked to the propargylic moiety. Initially, benzo[*d*][1,3]dioxol-5-ol **1** was treated with propargyl bromide (3-Bromoprop-1-yne) and sodium carbonate (Na_2CO_3) in acetonitrile to obtain 5-(prop-2-yn-1-yloxy) benzo[*d*][1,3]dioxole **3** in 90% yield after 4 hours (Chen et al. 2015). Compound **3** started the Mannich reaction, which resulted in the ten distinct compounds (**4a–j**) shown in Table 1. Briefly, a catalytic amount of cuprous iodide (CuI) in DMSO, formaldehyde, and amine (2° amine) was applied to compound **3**. Stirring the components for 4 hours at room temperature resulted in 65–79% yields of the necessary compounds (**4a–j**) (Scheme 1).

High-resolution mass spectrometry (HRMS) and ^{1}H and ^{13}C NMR spectroscopy were used to characterize the novel compounds. The mass spectra were found to be in good agreement with estimated values and provided the right molecular ion peaks. The ^{1}H-NMR spectra revealed protons that corresponded to aliphatic amine protons and the OCH_2 moiety in the aliphatic region δ= 4.55–5.68 ppm. The singlet CH_2N protons appeared at about the region δ = 3.26–3.37 ppm, while the singlet H-2 protons appeared at about δ = 5.85 ppm. At δ = 6.35–6.65 ppm, all aromatic moieties displayed resonances. However, the ^{13}C NMR spectra displayed all of the synthesized compounds' distinctive signals, including several aliphatic peaks for the C-2 and aliphatic amine moieties. In the aromatic area, all aromatic moieties displayed distinct and accurate carbon signals. For the majority of the synthesized compounds, the two alkyne carbon atom peaks (79.0–83.0) are identifiable.

Table 1. Structures of synthesized novel 4-(benzo[*d*][1,3]dioxol-5-yloxy)-*N*,*N*-2-yn-1-amine.

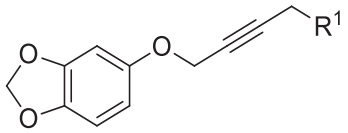

Compound	R1	Compound	R1
4a	*-N(CH3)2*	***4f***	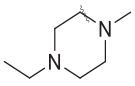
4b	*-N(CH2CH3)2*	***4g***	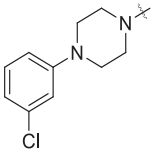
4c	*-N((CH2)2CH3)2*	***4h***	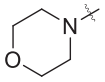
4d	*-N((CH2)3CH3)2*	***4i***	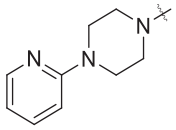
4e	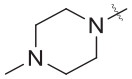	***4j***	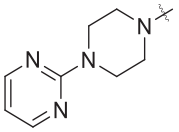

Molecular docking

This study investigated the potential of **4d** and **4g** compounds as antagonists for the CysLT2 receptor. To validate the docking procedure, the co-crystal structure, compound **11a**, was redocked, yielding an RMSD value of 0.98 Å, as represented in Fig. 12. It is proposed that RMSD values falling beneath the 2 Å limit validate the reliability of the docking protocol for subsequent examinations (Hevener et al. 2009). Table 2 shows the predicted binding affinities of the two compounds (**4d**, **4g**) against the CysLT2 receptor using molecular docking simulations.

Compound **4d** exhibited a binding energy of -6.57 kcal/mol, with an IC_{50} value of 18.7 μM, indicating moderate binding affinity and inhibitory activity. In comparison, compound **4g** demonstrated a significantly lower binding energy of -8.50 kcal/mol and an IC_{50} of 15.5 μM, reflecting a stronger interaction with the receptor. However, both compounds showed less potent binding energy and higher IC_{50} values than the co-crystalized antagonist **11a**, which achieved a superior binding energy of -14.92 kcal/mol and an IC_{50} of 2.9 nM. These results suggest that while compounds **4d** and **4g** interact effectively with the receptor, they are less potent than **11a**, likely due to differences in binding modes and interaction profiles.

Detailed interaction analysis revealed differences in the amino acids involved in the binding of each compound. Compound **4d** formed hydrophobic interactions with Tyr119, Met201, Ala205, His270, Leu271, and Arg267 (Fig. 14). However, no hydrogen bonds or electrostatic interactions were observed, which might contribute to its relatively lower binding energy and potency compared to **4g** and **11a**. Compound **4g** displayed a more diverse interaction profile, forming hydrogen bonds with Arg94 and Leu190 and hydrophobic interactions with Tyr119, Met172, Leu173, Leu188, Leu198, and Met201. This expanded interaction network likely accounts for its enhanced binding energy relative to **4d** (Fig. 14). Co-crystalized antagonist **11a** (Fig. 13) exhibited the most extensive interaction profile. It formed hydrogen bonds with Lys37 and Tyr119, electrostatic pi-cation interaction with Arg267, and hydrophobic contacts with Tyr123 (T-shape aromatic interaction), Leu190, Leu198, Met201, Ile204, Ala205, and Leu271. The comprehensive interaction network explains its superior binding affinity and IC_{50} value.

The lower binding energy of **4g** compared to **4d** suggests that the additional hydrogen bonding and broader hydrophobic interaction network of **4g** play a critical role in enhancing its binding affinity. Conversely, the absence of hydrogen bonding and electrostatic interactions in **4d** limits its overall interaction strength, resulting in weaker binding. The

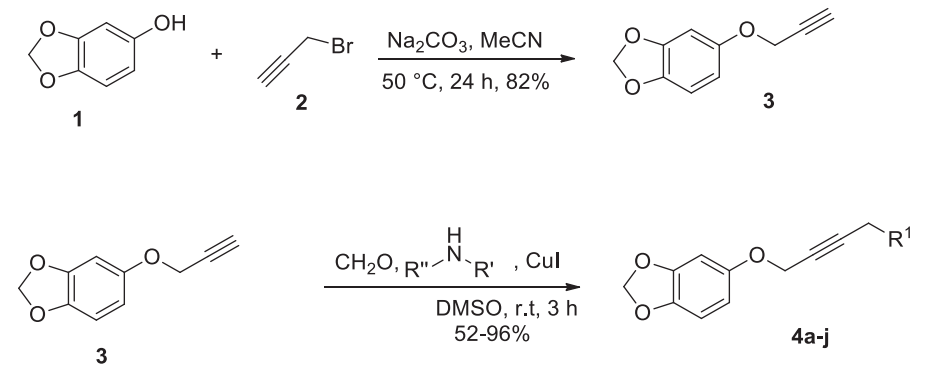

Scheme 1. Synthetic routes for the synthesis of 4-(benzo[*d*][1,3]dioxol-5-yloxy)-*N*,*N*-2-yn-1-amine pharmacophore hybrid.

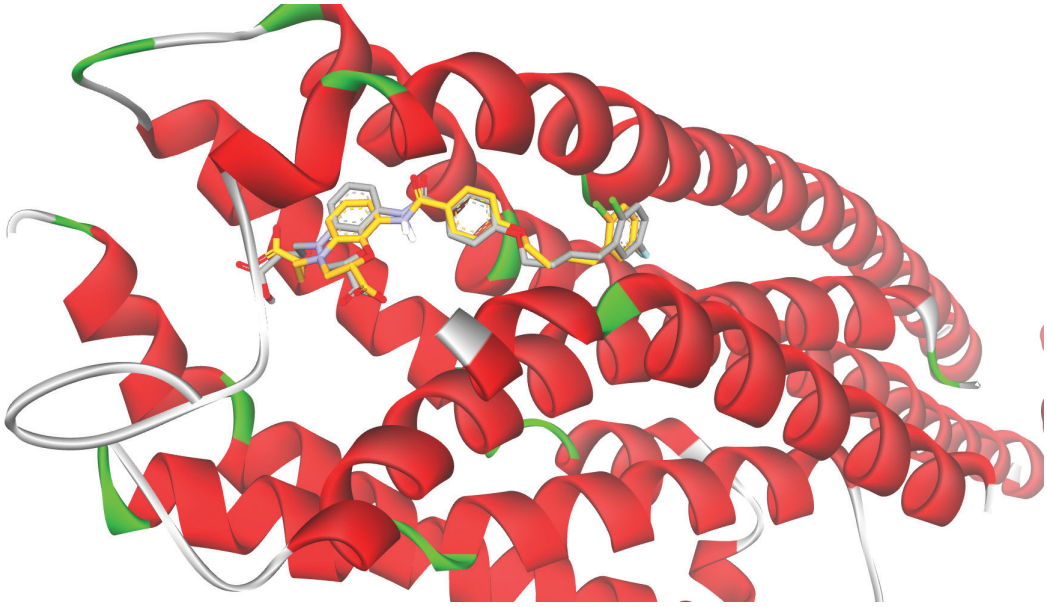

Figure 12. Stick representations of co-crystal structure Compound **11a** (gray) color and the docked configurations (orange) against the CysLT2 receptor (PDB ID: 6RZ6). Generated by Biovia Discovery Studio Visualizer®.

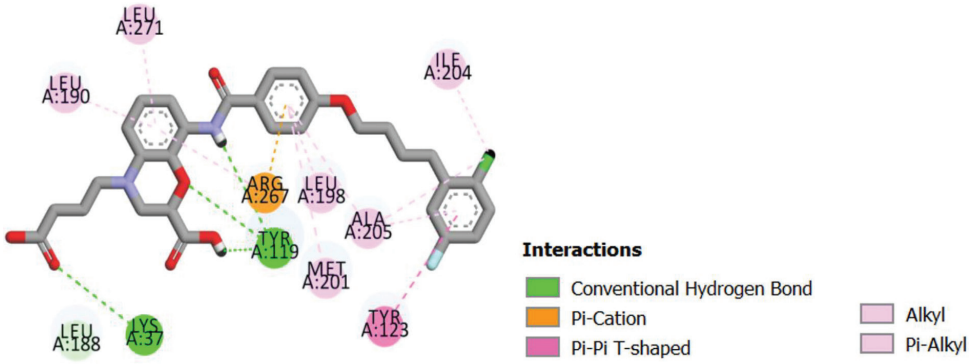

Figure 13. Stick representation of co-crystal structure compound **11a** within the CysLT2 receptor (PDB ID: 6RZ6) binding site. Generated by Biovia Discovery Studio Visualizer®.

Table 2. Lowest binding energy scores (Kcal/mol) for the co-crystal antagonist and the synthesized compounds **4d** and **4g** against the CysLT2 receptor.

Compound	Lowest Binding Energy (LBE) Kcal/mol	Tested IC_{50}	Interacting Amino Acids		
			H-Bond	Electrostatic	Hydrophobic
4d	-6.57	18.7 μM	ND	ND	Tyr119, Met201, Ala205, His270, Leu271, Arg267, Leu271
4g	-8.50	15.5 μM	Arg94, Leu190	ND	Tyr119, Met172, Leu173, Leu188, Leu198, Met201
11a (co-crystal structure)	-14.92	2.9 nM	Lys37, Tyr119	Arg267 (pi-cation)	Tyr123 (T-shape), Leu190, Leu198, Met201, Ile204, Ala205, leu271.

co-crystal antagonist **11a** remains the benchmark compound due to its extensive interaction network, which includes multiple hydrogen bonds, pi-cation electrostatic interactions, and hydrophobic contacts. The synthesized compounds, though promising, require further structural optimization to improve their interaction profiles and potency.

Evaluation of biological activities

We assessed the cytotoxic activities of the prepared compounds against cysteineyl leukotrienes (CysLT2) antagonists. Notably, Table 3 shows the inhibitory profiles of **4a-j**. Clearly, **4c** and **4g** have superior inhibitory percentages compared to other compounds, prompting us to pursue their IC_{50} values. Fig. 15 shows the resulting dose/response curves and IC_{50} values.

Table 3. Percent inhibition values of CysLT2 at 10 μM concentration of the prepared compounds.

Compound	% Inhibition at 10 μM[a]	IC_{50} (μM)
4a	10	ND[b]
4b	20	ND[b]
4c	14	ND[b]
4d	56	18.7
4e	8	ND[b]
4f	7	ND[b]
4g	54	15.5
4h	5	ND[b]
4i	6	ND[b]
4j	6	ND[b]
11a[c]	IC_{50} = 2.9 nM	

[a] Average of duplicate measurements ± standard deviation,
[b] ND: Not determined.
[c] Standard inhibitor (Gusach, A. et al. 2019).

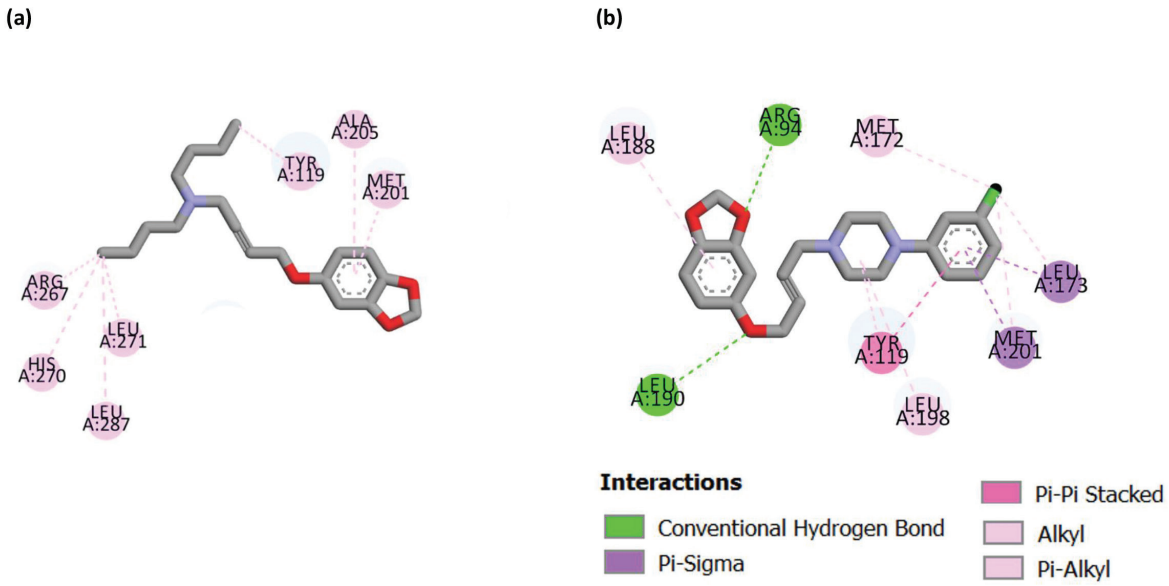

Figure 14. Stick representation of **a. 4d** and **b. 4g** docked within the CysLT2 receptor (PDB ID: 6RZ6) binding site. Generated by Biovia Discovery Studio Visualizer®.

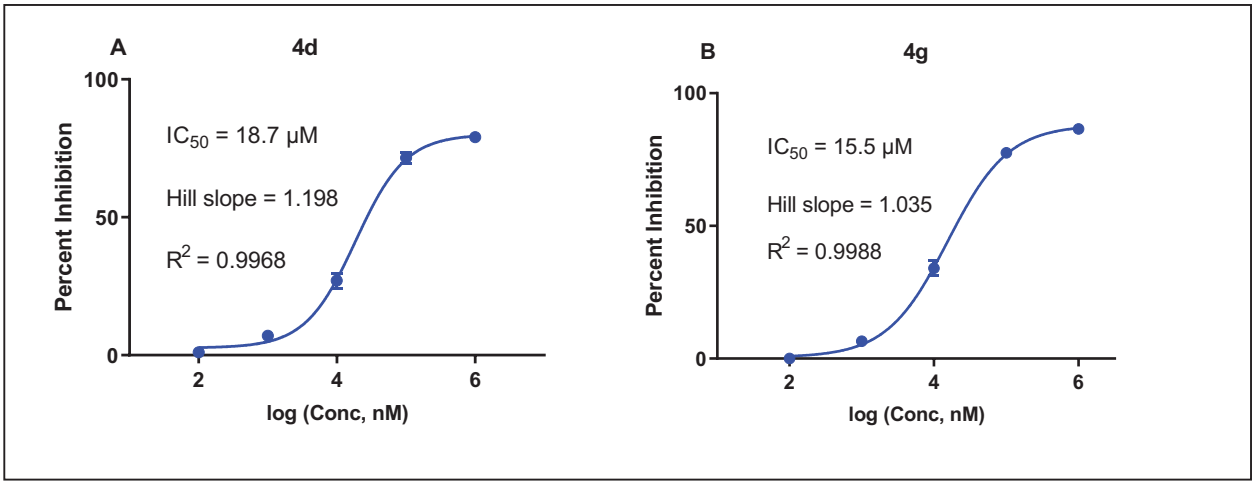

Figure 15. Dose-response curves of compounds **4d** and **4g** CysLT2 antagonist. **A.** Dose-response curve of **4d** with IC_{50} = 18.7 μM; **B.** Dose-response curve of **4g** with IC_{50} = 15.5 μM.

Conclusion

This study investigates a novel series of compounds featuring benzo[*d*][1,3]dioxol-5-ol as Cysteinyl Leukotriene (CysLT) antagonists. These compounds were synthesized through the direct reaction of 5-(prop-2-yn-1-yloxy) benzo[*d*][1,3]dioxole with various secondary aliphatic amines. In vitro evaluations indicated that, while all compounds displayed weak inhibitory activity against CysLT2, compounds **4d** and **4g** showed notable IC_{50} values of 18.7 μM and 15.5 μM, respectively.

Molecular docking studies further revealed differences in binding energy and interaction profiles between the synthesized compounds (**4d** and **4g**) and the co-crystallized antagonist (Compound **11a**). Although **4g** exhibited better binding affinity than **4d**, neither matched the binding potency of Compound **11a**. These findings highlight the need for further structural optimization to enhance the binding strength and inhibitory efficacy of the synthesized compounds against the CysLT2 receptor.

Introducing functional groups capable of forming additional hydrogen bonds or electrostatic interactions could significantly improve their binding affinity and potency. This study provides a valuable foundation for the rational design of more potent CysLT2 receptor inhibitors in future research.

Additional information

Conflict of interest

The authors have declared that no competing interests exist.

Ethical statements

The authors declared that no clinical trials were used in the present study.

The authors declared that no experiments on humans or human tissues were performed for the present study.

The authors declared that no informed consent was obtained from the humans, donors or donors' representatives participating in the study.

The authors declared that no experiments on animals were performed for the present study.

The authors declared that no commercially available immortalised human and animal cell lines were used in the present study.

Funding

No funding was reported.

Author contributions

All authors have contributed equally.

Author ORCIDs

Areej M. Jaber https://orcid.org/0000-0002-2991-1858
Mohammed M. Al-Mahadeen https://orcid.org/0009-0004-0130-7458
Belal O. Al-Najjar https://orcid.org/0000-0001-6811-1792
Raed A. Al-Qawasmeh https://orcid.org/0000-0002-9325-6229

Data availability

All of the data that support the findings of this study are available in the main text or Supplementary Information.

References

Al-Anazi M, Khairuddean M, O. Al-Najjar B, Murwih Alidmat M, Nur Syazni Nik Mohamed Kamal N, Muhamad M (2022) Synthesis, anticancer activity and docking studies of pyrazoline and pyrimidine derivatives as potential epidermal growth factor receptor (EGFR) inhibitors. Arabian Journal of Chemistry 15: 103864. https://doi.org/10.1016/j.arabjc.2022.103864

Al-Mahadeen MM, Jaber AM (2024) Comparative Studies of Benzimidazoles Synthetic Routes and its Biological Activity. Mini-Reviews in Organic Chemistry 21: 1–16. https://doi.org/10.2174/0118756298334834240828041219

Al-Mahadeen MM, Jaber AM, Al-Najjar BO (2024a) Design, synthesis and biological evaluation of novel 2-hydroxy-1 H-indene-1, 3 (2 H)-dione derivatives as FGFR1 inhibitors. Pharmacia 71: 1–9. https://doi.org/10.3897/pharmacia.71.e122127

Al-Mahadeen MM, Jaber AM, Al-Qawasmeh RA, Taha MO (2024b) Synthesis, evaluation, and docking study of adamantyl-1, 3, 4-oxadiazol hybrid compounds as CaMKIIδ kinase inhibitor. Journal of Chemical Research 48: 17475198241262467. https://doi.org/10.1177/17475198241262467

Al-Mahadeen MM, Jaber AM, Zahra JA, Al-Najjar BO, El-Abadelah MM, Khanfar MA (2025) Discovery and Chemical Exploration of Spiro[Benzofuran-3,3'-Pyrroles] Derivatives as Innovative FLT3 Inhibitors for Targeting Acute Myeloid Leukemia. Anti-Inflammatory & Anti-Allergy Agents in Medicinal Chemistry 24: 127–138. https://doi.org/10.2174/0118715230343474241009112335

Al-Mahadeen MM, Jaber AM, Zahra JA, El-Abadelah MM, Alshaer W, Taha MO (2024c) Synthesis of novel benzothieno-[3, 2'-f][1, 3] oxazepines and their isomeric 2-oxo-2 H-spiro [benzothiophene-3, 3'-pyrrolines] via 1, 4-dipolar cycloaddition reaction and their evaluation as cytotoxic anticancer leads. Medicinal Chemistry Research: 1–12. https://doi.org/10.1007/s00044-024-03229-9

Al-Mahadeen MM, Jaber MA, Al-Najjar OB, Khanfar AM, El-Abadelah MM (2024d) Novel N-Substituted Isatin-Oxoindolin-1H-Benzo[D] Imidazole Fumarate as a New Class of JNK3 Inhibitor: Design, Synthesis, Molecular Modeling and its Biological Activity. Current Organic Synthesis 21: 1–9. https://doi.org/10.2174/0115701794335274240910111137

Al-Mahadeen MM, Zahra JA, El-Abadelah MM, Jaber AM, Khanfar MA (2022) One-pot synthesis of novel 2-oxo(2H)-spiro[benzofuran-3,3'-pyrrolines] via 1,4-dipolar cycloaddition reaction. Results in Chemistry 4: 100643. https://doi.org/10.1016/j.rechem.2022.100643

Assab MA, Hasan HE, Alhamad H, Albahar F, Alzayadneh A, Assab HA, Dayyih WA, Zakaraya Z (2024) Assessing pharmacists' awareness of financial indicators in community pharmacy management: A cross-sectional study. Heliyon 10: e33338. https://doi.org/10.1016/j.heliyon.2024.e33338

Chen Y-Y, Chen K-L, Tyan Y-C, Liang C-F, Lin P-C (2015) Synthesis of substituted 3-methylene-2, 3-dihydrobenzofurans and 3-methylbenzofurans by rhodium (II)-catalyzed annulation. Tetrahedron 71: 6210–6218. https://doi.org/10.1016/j.tet.2015.06.075

Dassault-Systèmes (2016) Biovia, discovery studio modeling environment. 16.1 ed. Dassault Systèmes Biovia, San Diego, CA, USA.

Dayyih WA, Al-Ani I, Hailat M, Alarman SM, Zakaraya Z, Assab MA, Alkhader E (2024) Review of grapefruit juice-drugs interactions mediated by intestinal CYP3A4 inhibition. Journal of Applied Pharmaceutical Science 14: 059–068.

Gelosa P, Colazzo F, Tremoli E, Sironi L, Castiglioni L (2017) Cysteinyl Leukotrienes as Potential Pharmacological Targets for Cerebral Diseases. Mediators of Inflammation 2017: 3454212. https://doi.org/10.1155/2017/3454212

Gusach A, Luginina A, Marin E, Brouillette RL, Besserer-Offroy É, Longpré J-M, Ishchenko A, Popov P, Patel N, Fujimoto T, Maruyama T, Stauch B, Ergasheva M, Romanovskaia D, Stepko A, Kovalev K, Shevtsov M, Gordeliy V, Han GW, Katritch V, Borshchevskiy V, Sarret P, Mishin A, Cherezov V (2019) Structural basis of ligand selectivity and disease mutations in cysteinyl leukotriene receptors. Nature Communications 10: 5573. https://doi.org/10.1038/s41467-019-13348-2

Hevener KE, Zhao W, Ball DM, Babaoglu K, Qi J, White SW, Lee RE (2009) Validation of molecular docking programs for virtual screening against dihydropteroate synthase. Journal of Chemical Information and Modeling 49: 444–460. https://doi.org/10.1021/ci800293n

Jaber AM, Al-Mahadeen MM, Al-Qawasmeh RA, Taha MO (2023a) Synthesis, anticancer evaluation and docking studies of novel adamantanyl-1, 3, 4-oxadiazol hybrid compounds as Aurora-A kinase inhibitors. Medicinal Chemistry Research 32: 2394–2404. https://doi.org/10.1007/s00044-023-03145-4

Jaber AM, Zahra JA, El-Abadelah MM, Sabri SS, Khanfar MA, Voelter W (2020) Utilization of 1-phenylimidazo[1,5-a]quinoline as partner in 1,4-dipolar cycloaddition reactions. Zeitschrift für Naturforschung B 75: 259–267. https://doi.org/10.1515/znb-2019-0150

Jaber AM, Zahra JA, El-Abadelah MM, Sabri SS, Sabbah DaS (2023b) Thermodynamic control synthesis of spiro[oxindole-3,3'-pyrrolines] via 1,4-dipolar cycloaddition utilizing imidazo[1,5-a]quinoline. Zeitschrift für Naturforschung C 78: 141–148. https://doi.org/10.1515/znc-2022-0085

Jaber AM, Zahra JA, Sabri SS, Khanfar MA, Awwadi FF, El-Abadelah MM (2022) New Trends in 1, 4-Dipolar Cycloaddition Reactions. Thermodynamic Control Synthesis of Model 2'-(isoquinolin-1-yl)-spiro [oxindole-3, 3'-pyrrolines]. Current Organic Chemistry 26: 542–549. https://doi.org/10.2174/1385272826666220221141306

Jaber MA, Zahra AJ, El-Abadelah MM, Al-Mahadeen MM, Sabri SS, Kasabri V, Haddadin NR (2024) Evaluation of Spirooxindole-3,3'-pyrrolines-incorporating Isoquinoline Motif as Antitumor, Anti-Inflammatory, Antibacterial, Antifungal, and Antioxidant Agents. Anti-Inflammatory & Anti-Allergy Agents in Medicinal Chemistry 23: 1–12. https://doi.org/10.2174/0118715230322113240705071750

Jayaraj P, Narasimhulu CA, Rajagopalan S, Parthasarathy S, Desikan R (2020) Sesamol: a powerful functional food ingredient from sesame oil for cardioprotection. Food Funct 11: 1198–1210. https://doi.org/10.1039/C9FO01873E

Jo-Watanabe A, Okuno T, Yokomizo T (2019) The Role of Leukotrienes as Potential Therapeutic Targets in Allergic Disorders. International Journal of Molecular Sciences 20: 3580. https://doi.org/10.3390/ijms20143580

Kushwaha P, Singh N, Amresh G, Prakash O, Swarup S, Usmani S (2020) Phytochemical and Pharmacological Insight on Sesamol: An Updated Review. Current Bioactive Compounds 16: 1–8.

Lu J, Fan Y, Sha F, Li Q, Wu X-Y (2019) Copper-catalyzed enantioselective Mannich reaction between N-acylpyrazoles and isatin-derived ketimines. Organic Chemistry Frontiers 6: 2687–2691. https://doi.org/10.1039/C9QO00575G

Majdalawieh AF, Mansour ZR (2019) Sesamol, a major lignan in sesame seeds (Sesamum indicum): Anti-cancer properties and mechanisms of action. European Journal of Pharmacology 855: 75–89. https://doi.org/10.1016/j.ejphar.2019.05.008

Morris GM, Huey R, Lindstrom W, Sanner MF, Belew RK, Goodsell DS, Olson AJ (2009) AutoDock4 and AutoDockTools4: Automated docking with selective receptor flexibility. J Comput Chem 30: 2785–2791. https://doi.org/10.1002/jcc.21256

Parravicini C, Abbracchio MP, Fantucci P, Ranghino G (2010) Forced unbinding of GPR17 ligands from wild type and R255I mutant receptor models through a computational approach. BMC Structural Biology 10: 1–18. https://doi.org/10.1186/1472-6807-10-8

Ren B, Yuan T, Diao Z, Zhang C, Liu Z, Liu X (2018) Protective effects of sesamol on systemic oxidative stress-induced cognitive impairments via regulation of Nrf2/Keap1 pathway. Food Funct 9: 5912–5924. https://doi.org/10.1039/C8FO01436A

Sadybekov AA, Brouillette RL, Marin E, Sadybekov AV, Luginina A, Gusach A, Mishin A, Besserer-Offroy É, Longpré J-M, Borshchevskiy V (2020) Structure-based virtual screening of ultra-large library yields potent antagonists for a lipid GPCR. Biomolecules 10: 1634. https://doi.org/10.3390/biom10121634

Sahar Jaffal SO, Mohammad Alsalem, Belal Al-Najjar, (2022) Effect of *Arbutus andrachne* L. methanolic leaf extract on TRPV1 function: Experimental and molecular docking studies 12(10): 069–077. https://doi.org/10.7324/JAPS.2022.121007

Sekioka T, Kadode M, Fujii M, Kawabata K, Abe T, Horiba M, Kohno S, Nabe T (2015) Expression of CysLT2 receptors in asthma lung, and their possible role in bronchoconstriction. Allergology International 64: 351–358. https://doi.org/10.1016/j.alit.2015.04.008

Sood R, Anoopkumar-Dukie S, Rudrawar S, Hall S (2024) Neuromodulatory Effects of Leukotriene receptor antagonists: A comprehensive review. European Journal of Pharmacology: 176755. https://doi.org/10.1016/j.ejphar.2024.176755

Voisin T, Perner C, Messou MA, Shiers S, Ualiyeva S, Kanaoka Y, Price TJ, Sokol CL, Bankova LG, Austen KF, Chiu IM (2021) The CysLT(2) R receptor mediates leukotriene C(4)-driven acute and chronic itch. Proceedings of the National Academy of Sciences of the United States of America 118. https://doi.org/10.1073/pnas.2022087118

Zhou L, Zhang J, Han X, Fang J, Zhou S, Lu L, Shi Q, Ying H (2022) CysLT(2)R Antagonist HAMI 3379 Ameliorates Post-Stroke Depression through NLRP3 Inflammasome/Pyroptosis Pathway in Gerbils. Brain Sciences 12. https://doi.org/10.3390/brainsci12080976

Supplementary material 1

Supplementary data

Authors: Areej M. Jaber, Mohammed M. Al-Mahadeen, Belal O. Al-Najjar, Raed A. Al-Qawasmeh

Data type: docx

Link: https://doi.org/10.3897/pharmacia.72.e143171.suppl1